

Aerosol particle formation in the upper residual layer

Authors:

Janne Lampilahti¹, Katri Leino¹, Antti Manninen², Pyry Poutanen¹, Anna Franck¹, Maija Peltola¹, Paula Hietala¹, Lisa Beck¹, Lubna Dada¹, Lauriane Quéléver¹, Ronja Öhrnberg¹, Ying Zhou³, Madeleine Ekblom¹, Ville Vakkari^{2,4}, Sergej Zilitinkevich^{*}, Veli-Matti Kerminen¹, Tuukka Petäjä^{1,5}, Markku Kulmala^{1,3,5}

Affiliations:

¹Institute for Atmospheric and Earth System Research / Physics, Faculty of Science, University of Helsinki, Helsinki, Finland.

²Finnish Meteorological Institute, Helsinki, Finland.

³Aerosol and Haze Laboratory, Beijing Advanced Innovation Center for Soft Matter Science and Engineering, Beijing University of Chemical Technology, Beijing, China.

⁴Atmospheric Chemistry Research Group, Chemical Resource Beneficiation, North-West University, Potchefstroom, South Africa.

⁵Joint International Research Laboratory of Atmospheric and Earth System Sciences, Nanjing University, Nanjing, China.

Correspondence to: Janne Lampilahti (janne.lampilahti@helsinki.fi)

Abstract: According to current estimates, atmospheric new particle formation (NPF) produces a large fraction of aerosol particles and cloud condensation nuclei in the earth's atmosphere, therefore having implications for health and climate. Despite recent advances, atmospheric NPF is still insufficiently understood in the lower troposphere, especially above the mixed layer (ML). This paper presents new results from co-located airborne and ground-based measurements in a boreal forest environment, showing that many NPF events (~42%) appear to start in the topmost part of the RL. The freshly formed particles may be entrained into the growing mixed layer (ML) where they continue to grow in size, similar to the aerosol particles formed within the ML. The results suggest that in the boreal forest environment, NPF in the upper RL has an important contribution to the aerosol load in the BL.

1. Introduction

It has been estimated that atmospheric new particle formation (NPF) is responsible for most of the cloud condensation nuclei (CCN) in the atmosphere (Dunne et al., 2016; Gordon et al., 2017; Pierce and Adams, 2009; Yu and Luo, 2009). Aerosol-cloud interactions, in turn, have important but poorly-understood effects on climate (Boucher et al., 2013). Being a major source of ultrafine aerosol particles in many environments (e.g. Brines et al., 2015; Posner and Pandis, 2015; Salma et al., 2017; Yu et al., 2019), NPF may have implications for human health.

* Deceased Feb 15, 2021

41 NPF has been observed in various environments and at various altitudes inside the troposphere. The
42 majority of NPF observations come from ground-based measurements (Kerminen et al., 2018;
43 Kulmala et al., 2004), which can be argued to represent NPF within the mixed layer (ML). ML is a
44 type of atmospheric BL where turbulence uniformly, especially vertically, mixes quantities like
45 aerosol particle concentrations. Measurements from aircrafts show that NPF is also common in the
46 upper free troposphere (FT) (e.g. Clarke and Kapustin, 2002; Takegawa et al., 2014). Entrainment
47 of particles formed in the upper FT was identified as an important source of CCN in the tropical
48 boundary layer (BL) (Wang et al., 2016; Williamson et al., 2019). Measurements from high-altitude
49 research stations also demonstrate that NPF frequently takes place in the FT, in these cases NPF was
50 often observed in BL air that was transported to the higher altitudes (Bianchi et al., 2016; Boulon et
51 al., 2011; Rose et al., 2017; Venzac et al., 2008).

52

53 When studying the vertical distribution of NPF in the lower troposphere one has to consider the
54 evolution and dynamics of the BL. Nilsson et al. (2001) found that the onset of turbulent mixing
55 correlated better with the onset of NPF at ground level than with the increase in solar radiation. The
56 authors gave several hypotheses to why this might be. One hypothesis was that NPF starts aloft,
57 either in the RL or in the inversion capping the shallow morning ML. As the turbulent mixing starts,
58 the newly formed particles would be transported down and observed at the ground-level.

59

60 Many observations have supported the hypothesis put forward by Nilsson et al. (2001). Größ et al.
61 (2018), Meskhidze et al. (2019) and Stanier et al. (2004) reported positive correlation between the
62 onset of NPF at ground level and the breakup of the morning inversion due to beginning of
63 convective mixing. Chen et al. (2018), Platis et al. (2015) and Siebert et al. (2004) used in situ
64 airborne measurements and observed that NPF started during the morning on the top of a shallow
65 ML capped by a temperature inversion at a few hundred meters above ground. The particles grew to
66 detectable nucleation mode (sub-25 nm) sizes aloft, and when the ML began to grow due to
67 thermally-driven convection, the particles were mixed downwards and observed at the ground-level
68 where they further continued to grow in size. Stratmann et al. (2003) observed newly formed
69 particles inside the RL disconnected from the shallow ML or the inversion that capped it.
70 Furthermore, Wehner et al. (2010) observed that NPF inside the RL was connected to turbulent
71 layers. On the other hand, Junkermann and Hacker (2018) attributed their observations of elevated
72 ultrafine particle layers at few hundred meter altitudes in the RL to flue gas emissions from
73 smokestacks with subsequent chemistry taking place during air mass transport over long distances.

74

75 The hypothesis proposed by Nilsson et al. (2001) was based on observations done in Hyytiälä,
76 Finland, which is a rural site surrounded by boreal forests and with very clean air. However, the
77 supporting evidence comes from measurements done in more polluted environments in Central
78 Europe and USA. Airborne measurements done over Hyytiälä have not found NPF on top of the
79 shallow morning ML or within the bulk of the RL, instead the NPF events seem to start within the
80 ML (Boy et al., 2004; Laakso et al., 2007; O’Dowd et al., 2009). This might be because in the more
81 polluted environments there are high enough concentrations of precursor vapors from
82 anthropogenic sources that NPF can be initiated in the morning inversion and/or within the bulk of
83 the RL. Interestingly, though, observations from Hyytiälä using a small instrumented airplane have
84 frequently found nucleation mode particle layers above the ML at a much higher altitude range of
85 ~1500-2800 m above ground and the explanation for these layers is not clear (Leino et al., 2019;
86 Schobesberger et al., 2013; Väänänen et al., 2016). For example Väänänen et al. (2016) found that
87 for the 2013-2014 airborne measurement campaigns 16/36 (~44%) profiles showed an elevated sub-
88 25 nm particle layer.

89
90 In this study we used co-located airborne and ground-based measurements to study nanoparticles
91 over a boreal forest in Hyytiälä, Finland. We aimed to characterize the elevated nucleation mode
92 particle layers that were a frequent observation in the previous studies. Specifically we were
93 looking at the following questions: (1) where in terms of atmospheric layers, how often and why do
94 these aerosol particle layer occur, and (2) how they are related to ground-based observations, and
95 what implications this has for data interpretation.

97 **2. Materials and methods**

99 ***2.1. Airborne measurements***

100
101 We used data from airborne measurement campaigns conducted between 2011 and 2018 around
102 Hyytiälä, Finland. Here we focused on data within 40 km radius from Hyytiälä. Figure 1 shows the
103 data availability from these measurements. Most of the flights were carried out during spring and
104 early autumn because that is when NPF events are most common in Hyytiälä. The measurement
105 setups changed slightly over the years. Detailed descriptions of the setups on board can be found in
106 previous studies (Leino et al., 2019; Schobesberger et al., 2013; Väänänen et al., 2016).

107

108 The instrumented aircraft was a Cessna 172 operated from the Tampere-Pirkkala airport (ICAO:
109 EFTP). The sample air was collected through an outside inlet into a main sampling line that was
110 inside the aircraft's cabin. The forward movement of the aircraft during flight provided adequate
111 flow rate inside the main sampling line. The flow rate was maintained at 47 lpm by using a manual
112 valve. The instruments drew air from the main sampling line using core sampling inlets. The
113 necessary flow rate to the instruments was provided by pumps. The airspeed was kept at 130 km/h
114 during the measurement flights.

115

116 The aerosol instruments on board considered in this study were an ultrafine condensation particle
117 counter (uCPC, TSI, model: 3776), measuring the >3 nm particle number concentration at a 1-s
118 time resolution, a particle size magnifier (PSM, Airmodus, model: A10) operated with a TSI 3010
119 CPC, measuring the >1.5 nm particle number concentration at a 1-s time resolution, and a custom-
120 built scanning mobility particle sizer (SMPS) with a short Hauke type DMA and a TSI 3010 CPC,
121 measuring the aerosol number size distribution in the size range of 10-400 nm. The time resolution
122 of the SMPS was about 2.2 min. In addition, basic meteorological data (temperature, relative
123 humidity and pressure) and water vapor concentration from Licor Li-840 gas analyzer were used.

124

125 Vertically, the measurement profiles extended approximately from 100 m to 3000 m above the
126 ground. This altitude range covered the ML, RL and roughly 1 km of the FT (Figure 2). The
127 measurement flights lasted about 2-3 hours and were flown mostly during the morning (~6:00-
128 10:00 UTC) and afternoon (~11:00-14:00 UTC). Horizontally, the profiles were flown
129 perpendicular to the mean wind in order to avoid the airplane's exhaust fumes.

130

131 **2.2. Ground-based measurements**

132

133 Comprehensive atmospheric measurements have been done at the SMEAR II station in Hyytiälä
134 (61°50'40" N, 24°17'13" E, 180 m above sea level) since 1996 (Hari and Kulmala, 2005). The
135 landscape around the site is flat and dominated by Scots pine forests, with small farms and lakes
136 scattered nearby. The station represents typical rural background conditions.

137

138 We used data from the BA ECC (Biogenic Aerosols–Effects on Clouds and Climate) campaign,
139 which took place in Hyytiälä during Feb-Sep, 2014 (Petäjä et al., 2016), to study the relationship
140 between BL evolution and NPF observed at the station. High spectral resolution lidar (HSRL)
141 measurements and meteorological balloon soundings released every 4 hours by the U.S. Department

142 of Energy ARM mobile facility allowed us to monitor the evolution of the BL (Nikandrova et al.,
143 2018).

144

145 From the HSRL data we looked at the values of backscatter cross section in order to see the
146 development of the ML during the day. The data were averaged into 30-m altitude bins and 10-min
147 temporal bins. The ground-based measurements during the BAECC campaign were also
148 supplemented by aircraft measurements using the instrumented Cessna. In case of missing
149 soundings, we also looked at the balloon soundings released from Jokioinen ~120 km south-west
150 from Hyytiälä (WMO: 02963).

151

152 The number size distribution of aerosol particles between 3 and 1000 nm was measured at the
153 station using a differential mobility particle sizer (DMPS, Aalto et al., 2001). A neutral cluster and
154 air ion spectrometer (NAIS, Airel Ltd., Mirme and Mirme, 2013) measured the number size
155 distribution of air ions and particles in the size ranges of 0.8-42 nm and 2-42 nm, respectively
156 (Manninen et al., 2009). The time resolutions of the DMPS and NAIS were 10 min and 4 min,
157 respectively. The vertical flux of particles >10 nm was measured by the eddy covariance method
158 from 23 m above ground, which is a couple of meters above the canopy (Buzorius et al., 2000). The
159 growth rates for aerosol particles were calculated using the log-normal mode fitting method
160 described in (Kulmala et al., 2012).

161

162 Vertical profiles of horizontal and vertical winds were measured with a Halo Photonics Stream Line
163 scanning Doppler lidar since year 2016. The Halo Photonics Stream Line is a 1.5 μm pulsed
164 Doppler lidar with a heterodyne detector and 30-m range resolution, and the minimum range of the
165 instrument is 90 m (Pearson et al., 2009). At Hyytiälä, a vertical stare of 12 beams and integration
166 time of 40 s per beam is scheduled every 30 min, whereas the other scan types operated during the
167 30-min measurement cycle were not utilized in this study. The lidar data were corrected for a
168 background noise artifact (Vakkari et al., 2019). The turbulent kinetic energy (TKE) dissipation rate
169 was calculated from the vertical stare according to the method by O'Connor et al. (2010) with a
170 signal-to-noise-ratio threshold of 0.001 applied to the data. Data availability is limited by relatively
171 low aerosol concentration at Hyytiälä, but TKE dissipation rate can be retrieved on most days up to
172 the top of the BL.

173

174 **3. Results and discussion**

175

176 In the airborne measurements we frequently observed a layer of nucleation mode (sub-25 nm)
177 particles above the ML. First we introduce how the phenomenon was observed in the airborne and
178 ground-based measurements using two case studies. Then we show that sub-25 nm particle layers
179 occurred in the topmost part of the RL by studying the average vertical profile of particle number-
180 size distribution and temperature from the airplane. Then we associate the nucleation mode particles
181 in the upper RL to a specific signal in the ground-based measurements and use the observations at
182 the SMEAR II station to gather long-term statistics. All times are reported in UTC.

183

184 **3.1 Case study: May 2, 2017**

185

186 On May 2, 2017 during the measurement airplane's ascend over Hyytiälä we observed an increased
187 number concentration of 3-10 nm (N_{3-10}) and 1.5-3 nm ($N_{1.5-3}$) particles, approximately between
188 1200 and 2000 m above sea level (asl), in the top parts of the ML (Figure 3A). The lower edge of
189 the aerosol particle layer was observed at 12:24. Within the particle layer the maximum $N_{1.5-3}$ was
190 $\sim 5000 \text{ cm}^{-3}$ and N_{3-10} was $\sim 6000 \text{ cm}^{-3}$. Below the particle layer $N_{1.5-3}$ and N_{3-10} were $\sim 3000 \text{ cm}^{-3}$.
191 Above the layer N_{3-10} dropped to $\sim 200 \text{ cm}^{-3}$. This low number concentration indicates that the
192 airplane was measuring above the ML. The $N_{1.5-3}$ dropped to $\sim 2000 \text{ cm}^{-3}$ and further down to ~ 200
193 cm^{-3} during the descend. The temperature inversion and the drop in water vapor concentration
194 indicate that the height of the ML was approximately 2200 m asl (Figure 3B).

195

196 The PSM sometimes had problems with increasing background number concentration (measured
197 with a filter in front of the inlet) during ascends, especially above 2 km. In these cases the
198 background number concentration would increase as the altitude was increased. It is unlikely that
199 on this day the $N_{1.5-3}$ layer was caused by this kind of instrumental problem alone because the
200 number concentration decreased above the layer.

201

202 During the descend the airplane entered back into the ML at 12:56 and the $N_{1.5-3}$ and N_{3-10} were
203 increased throughout the ML. The $N_{1.5-3}$ was around 4000 cm^{-3} and N_{3-10} increased from 4000 cm^{-3} to
204 around 8000 cm^{-3} towards the surface. On the same day, an early morning flight before the sunrise
205 was also performed (Figure 3A). During this flight no elevated aerosol particle layer was observed
206 and the number concentrations were quite uniform with altitude in the different size ranges, staying
207 below 1500 cm^{-3} .

208 |

209 | Roughly 10 min after the aerosol particle layer was first observed from the airplane during the
210 ascend, a new particle mode with similar-sized particles (geometric mean mode diameter about 10
211 nm) appeared at the ground-level at 12:36 (Figure 3C). This time was estimated from the NAIS
212 measurements. The appearance of this new particle mode was characterized by a negative peak in
213 the vertical particle flux, suggesting that the particles could be mixed down from aloft. The new
214 particle mode continued to grow for several hours despite the airmass moving over Hyytiälä,
215 indicating a large horizontal source area for the particles. At the ground level a new particle mode
216 with lower number concentration coupled with negative particle flux also appeared at around 10:00.
217

218 The number concentration of >3 nm aerosol particles along the afternoon flight track is shown in
219 Figure 3D. The particle layer was observed roughly 4 km north of Hyytiälä. Throughout the flight
220 the particle number concentration was higher in the north compared to the south. To take this
221 horizontal variability into account we only included aerosol data from the northern part of the flight
222 track in Figure 3A. The particle layer could still appear in the airborne data and later in the ground-
223 based data if the particles were transported from north to south during the measurement period due
224 to a change in wind direction. Wind measurements from the SMEAR II mast at 67.2 m altitude
225 show that the wind direction changed from 290 degrees to 330 degrees between 12:00-12:30
226 (Figure 3E). The particles were observed at the SMEAR II station right after the wind direction had
227 changed. On the other hand the negative particle flux associated with the appearance of the particles
228 would suggest an elevated source and in the case of airmass change we would expect to see the
229 particles appear during the change in wind direction, not after it. In any case it is difficult to say
230 conclusively if the aerosol particle observations on this day were due to vertical or horizontal
231 transport.

232
233 The airmasses came from the Arctic Ocean over northern Scandinavia. They went over the west
234 coast of Finland where there are known pollution sources, however in Hyytiälä the SO_2 and CO
235 levels remained low all day (~ 0.025 ppb and ~ 115 ppb for SO_2 and CO, respectively). Even when
236 the particles were observed at the measurement station no increase in pollutant concentrations was
237 observed. Pollution released into the night time RL from elevated sources such as flue gas stacks
238 would be expected to form layers at lower altitudes, below few hundred meters. If the pollution is
239 released during daytime, it is expected to be uniformly mixed into the ML and stay like that in the
240 RL (Junkermann and Hacker, 2018).

241

242 In order to study the atmospheric layers in the lower troposphere we plotted the TKE dissipation
243 rate calculated from the Doppler lidar measurements during May 1-2, 2017 and temperature
244 soundings from Jokioinen (Figure 3F). In the Doppler lidar measurements, the increase in the TKE
245 dissipation rate reveals the development of the ML on both days. On May 1, 2017 the ML reached
246 roughly 1900 m asl. The temperature sounding at 18:00 shows that this mixed layer was capped by
247 a thermal inversion at about 2000 m asl. In the two subsequent soundings during the night the
248 inversion stayed at roughly the same altitude and marked the top of the RL. In the temperature
249 sounding on May 2, 2017 at 12:00 only one inversion is observed at about 1900 m asl suggesting
250 that at this point the RL was already mixed into the growing ML. The lidar measurement agrees that
251 on May 2, 2017 the ML reached 1900 m asl around 12:00. About 25 min later the aerosol particle
252 layer was observed from the Cessna. These observations are supported by the temperature and water
253 vapor profiles measured on board the Cessna during the morning and afternoon flights (Figure 3B).

254

255 **3.2 Case study: May 19, 2018**

256

257 On May 19, 2018 a similar case was observed. Figure 4A shows that during the airplane's ascend
258 the lower edge of the particle layer was observed at ~1200 m asl and the top of the layer was at
259 2000 m asl. The N_{3-10} increased in the layer from ~1000 cm^{-3} up to ~10000 cm^{-3} . When the airplane
260 descended back into the ML the N_{3-10} was increased to around 6000 cm^{-3} throughout the ML. The
261 temperature and water vapor measurements show that a well-mixed layer was capped by inversion
262 at 2000 m asl (Figure 4B). Unfortunately the PSM was not working during this flight.

263

264 Figure 4C shows that horizontally the particle layer was observed approximately 5 km west of the
265 SMEAR II station. When the airplane entered back into the ML the particle number concentration
266 was increased over the SMEAR II station and in the west part of the measurement area. The aircraft
267 only flew ~2 km east of the SMEAR II station before turning southwest towards the airport, so it is
268 unclear if the number concentration was increased in the east as well. There was no appreciable
269 change in wind direction, which was from the north, during the measurement period (Figure 4D).
270 Therefore it is unlikely that the particles in the layer were horizontally transported to Hyytiälä from
271 west to east.

272

273 The air masses arrived from a similar sector as in the May 2, 2017 case (Arctic Ocean over northern
274 Scandinavia). SO_2 and CO concentrations in Hyytiälä remained low during the measurements
275 (~0.05 ppb and ~127 ppb for SO_2 and CO, respectively).

276

277 Figure 4E shows particle number size distribution measurements from the measurement airplane
278 and from the field station. The particle layer was observed as increased number concentrations in
279 the smallest size channels of the SMPS at 9:00 before the airplane flew above the ML. Roughly 20
280 minutes later a similar-sized particle mode appeared in the ground-based data. For this day there
281 were no particle flux data. The new particle mode continued to grow larger inside the ML for
282 several hours.

283

284 Figure 4F shows the TKE dissipation rate on May 18-19, 2018 from Hyytiälä and temperature
285 soundings from Jokioinen. On May 18, 2018 the ML went up to 2500 m asl in Hyytiälä. The
286 Jokioinen soundings show that at 6:00 the top of the RL was at about 1800 m asl, marked by the
287 subsiding inversion left from the previous day's ML. The top of the particle layer was at
288 approximately 2000 m asl.

289

290 | ***3.4 Evidence of nanoparticles in the upper RL based on long-term airborne measurements***

291 |

292 In the two case studies above the aerosol particle layer was associated with the altitude where the
293 top of the RL was. In order to study this connection further we analyzed the airborne data measured
294 during 2011-2018. In Figure 5 we plotted the median and 75th percentile number size distributions
295 measured on board the aircraft as a function of altitude during NPF event days (65 days out of 130
296 measurement days) between 07:00 and 10:00 UTC. This is the time window when the morning
297 measurement flight was usually done. NPF event days are characterized by a new growing particle
298 mode appearing in the sub-25 nm size range (Dal Maso et al., 2005). If aerosol formation in the
299 upper RL occurs on less than half of the NPF event days, it might not be visible in the median plot,
300 but might still appear in the 75th percentile plot.

301

302 Interestingly, in the 75th percentile plot a layer of nucleation mode particles is observed at 2500-
303 3000 m above sea level. This altitude range is well above the still growing ML at 07:00-10:00. We
304 wanted to know if the elevated particle layer was associated with a temperature inversion, since the
305 RL is commonly capped by such an inversion (Stull, 1988). In Figure 5 we plotted the mean
306 temperature profile from the flights when the N_{10-25} in 2000-3000 m altitude range exceeded the 75th
307 percentile N_{10-25} value (18 days).

308

309 The temperature profile shows an inversion base at 2500 m and this is likely where on average the
310 top of the RL was. The reason for the unusually deep RL is probably that the NPF event days tend
311 to be sunny spring days and the ML can grow exceptionally high, which also leads to a deep RL.
312 Our finding is in line with previous observations by Schobesberger et al. (2013) who measured
313 nucleation mode particles close to an elevated temperature inversion above the ML on multiple
314 measurement flights over southern Finland.

315

316 | ***3.5 Connection between nanoparticles in the upper RL and ground-based observations***

317 |

318 With the BAEC dataset we wanted to investigate whether the sudden appearance of nucleation
319 mode particles with downward particle flux was associated with the ML reaching the upper RL.
320 This would not only further test the hypothesis that the nanoparticles reside the topmost part of the
321 | RL, but also provide us with a condition to identify these events from the ground-based data alone.

322 |

323 We looked for cases where a new particle mode suddenly appeared in the nucleation mode size
324 range during the daytime and the first observation of these particles was associated with a negative
325 peak in particle flux. We noted the times when the particles first appeared, and also estimated a
326 confidence interval of the observation. Then we checked if we could find out the height of the RL
327 from balloon soundings or the Cessna flights. We looked for an elevated temperature inversion that
328 was roughly at the same altitude as the previous day's maximum ML height, which was determined
329 from HSRL and/or sounding. We noted the base height of the temperature inversion and took this as
330 the top of the RL. Then we followed the height of the new ML from the HSRL measurements and
331 noted the time when the ML reached the inversion base, also estimating a confidence interval.

332 | Figure 6 illustrates an example for this procedure.

333 |

334 We found 8 cases during the campaign where the analysis could be fully carried out and they are
335 summarized in Table 1. Figure 7 shows a positive correlation between the new particle mode
336 appearance time and the time when the ML reached the top of the RL. This suggests that the
337 suddenly appearing nucleation mode particles were entrained into the ML from the upper RL. We
338 found only a weak positive correlation between the new particle mode appearance time and the
339 geometric mean diameter of particles in the new mode at the moment they were first observed. The
340 mean growth rate of the appearing particle modes was 2.2 nm h^{-1} which is similar to 2.5 nm h^{-1}
341 reported by Nieminen et al. (2014) for 3-25 nm particles during NPF events in Hyytiälä.

342

343 The time that the ML reaches the upper RL depends on the height of the RL, which in turn depends
344 on the height of the ML on the previous day and the rate at which the top of the RL subsides. The
345 mixing time also depends on the rate at which the ML on the day of interest grows. For example on
346 March 28, 2014 the ML height on the previous day and the RL height during the night were 1300 m
347 and 1100 m, respectively. On April 4, 2014 the corresponding numbers were 2800 m and 2200 m.
348 Because of this on March 28, 2014 the ML reached the upper RL much earlier at ~7:00 compared to
349 April 4, 2014 when the ML reached the upper RL at ~11:00. For example on April 15, 2014 the ML
350 grew slowly in the morning due to presence of low clouds that limited convection. Because of this
351 the ML reached the top of the RL relatively late at 13:00.

352

353 In a well-mixed layer we would expect the entrained particles to reach the surface in less than an
354 hour (Stull, 1988). If the BL was stratified the particles could reach the surface at very different
355 rates which might significantly distort the results in Figure 7. The balloon soundings indicate that
356 the MLs in the 8 cases were well-mixed since the potential temperature profiles calculated from
357 soundings released around noon and late afternoon were almost constant up to the top of the ML
358 (see example profile in Figure 6).

359

360 ***3.6 Proposed explanation for the results***

361

362 One possible explanation for the elevated nucleation mode particle layers could be long-range
363 transport coupled with changes in the particle number size distribution such as particle shrinkage.
364 However, it is not clear why such process would favor the RL-FT interface. If the particle emissions
365 were released into the ML they would likely be distributed more or less uniformly throughout the
366 RL and not be concentrated at the top of the RL. If the transported particles subsided from the FT,
367 we would expect to see particle layers at various altitudes in the FT on different days, and the layers
368 would not be localized at the top of the RL. We studied the origin of the airmasses in the particle
369 layers and found that they were mostly coming from the so-called “clean sector” in the northwest of
370 Hyytiälä (Figure 8). During other than winter months this sector is associated with non-polluted air
371 and NPF from natural precursors (Tunved et al., 2006).

372

373 We find the most likely explanation to be NPF in the upper RL. The gaseous precursors involved in
374 NPF may end up in the upper RL because of mixing from the surface during the previous day (e.g.
375 organic vapors emitted from the forest or sulfuric acid, ammonia and amines originating from
376 human activities) or because of long-range transport in the FT (e.g. iodine oxides from the ocean).

378 Many factors favor NPF at higher altitudes, including enhanced photochemistry, reduced sinks and
379 reduced temperature. However, the NPF inducing features of the upper RL would probably be
380 linked to the mixing that takes place in the interface between the RL and FT, since this is the place
381 where the particle layers seem to be limited to. Nilsson and Kulmala, (1998) found that mixing two
382 air parcels with different initial temperatures and precursor vapor concentrations can lead to a
383 considerable increase in the nucleation rate. Therefore mixing air from the RL and FT over the
384 inversion, where the precursors are present in one of the layers (most likely the RL), could induce
385 aerosol particle formation in the interface layer.

386

387 Another possibility is that the RL and the FT contain different precursor vapors that did not initiate
388 nucleation or particle growth on their own, however when the vapors are mixed in the interface
389 between the two layers NPF occurs. For example on May 2, 2017 Beck et al. (in preparation)
390 measured the composition of naturally charged ions using a mass spectrometer on board an aircraft
391 concurrently with our measurements. It was found that during the first flight (~02:30-04:00 UTC)
392 the chemical composition was different in the RL compared to the FT. For example highly
393 oxygenated molecules (HOMs) as well as iodine containing compounds were present in the RL
394 while methanosulfonic acid (MSA) and sulfuric acid were detected in the FT.

395

396 If the growing ML reaches the upper RL, the newly formed particles will be mixed downwards into
397 the ML where they continue to grow in size as low-volatility vapors present in the ML are able to
398 condense onto these particles. The processes are illustrated in Figure 9. In case the particles will not
399 be mixed down, they may persist in the FT for a longer time period and possibly have stronger
400 contribution to cloud formation.

401

402 ***3.7 Implications for classifying NPF events***

403

404 Previous studies that classified NPF events observed in Hyytiälä have collected statistics on the
405 occurrence of suddenly appearing particle modes. Buenrostro Mazon et al. (2009) classified the so-
406 called undefined days between 1996-2006 from Hyytiälä. The undefined days are days that do not
407 fit the NPF event or the nonevent day classes (Dal Maso et al., 2005). One category the authors
408 used was “tail events” where a new particle mode appears at particle diameters greater than 10 nm
409 and grows for several hours. The authors found that 26% of NPF events were tail events (assuming
410 that tail events were also NPF events). Dada et al. (2018) collected statistics on “transported events”

411 where elevated number concentration of 7-25 nm particles persisted for more than 1.5 hours, but no
412 elevated number concentrations at smaller particle sizes were observed. It was found that 36% of
413 the NPF events observed for over 10 years in Hyytiälä were “transported events”. They occurred
414 especially when the conditions inside the ML were less favorable for nucleation.

415

416 Here we found cases in the SMEAR II data between 2013 and 2017, in which a new growing
417 particle mode suddenly, without continuous growth from smallest detectable sizes (3 nm), appears
418 in the nucleation mode (sub-25 nm) and is associated with a negative peak in the vertical particle
419 flux (upper RL NPF). We also noted cases where a new particle mode appears with a continuous
420 growth from the smallest detectable sizes (ML NPF). Based on the previous analysis we assume
421 that in the former case NPF took place in the upper RL and in the latter case inside the ML. The
422 analysis included 1750 days.

423

424 The monthly fractions of the different cases are shown in Figure 8. We found that NPF within the
425 ML occurred on 13% (234/1750) of all the days and NPF in the upper RL on 7% (117/1750) of all
426 the days. During spring (Mar-May) the corresponding percentages were 31% (132/431) and 17%
427 (74/431). On many days NPF took place both in the upper RL and within the ML (4% or 74/1750 of
428 all days and 12% or 53/431 of spring days). According to this analysis, NPF in the upper RL
429 constitutes 42% (117/277) of the NPF event days in Hyytiälä.

430

431 The monthly distribution of upper RL NPF events follows the distribution of ML NPF events, with
432 a peak during spring (Mar-May). This is well in line with previous studies that classified NPF
433 events in Hyytiälä (Dal Maso et al., 2005; Nieminen et al., 2014). This makes sense since the
434 conditions favoring ML NPF would also favor upper RL NPF. However, Buenrostro Mazon et al.
435 (2009) and Dada et al. (2018) found that the tail events and transported events had a peak during the
436 summer months (Jun-Aug).

437

438 On 16% of the NPF event days NPF only took place in the upper RL but not in the ML. This
439 number is smaller than the 36% found by Dada et al. (2018) for transported events and the 26%
440 found by Buenrostro Mazon et al. (2009) for tail events. This might be because we restricted to
441 cases where a negative peak in particle flux was associated with the appearance of nucleation mode
442 particles. For example, a case where the particles were horizontally advected to the measurement
443 site would not be expected to cause a negative peak in the particle flux and therefore would not be
444 classified as upper RL NPF.

445

446 **4. Conclusions**

447

448 We measured aerosol particles, trace gases and meteorological parameters on board an instrumented
449 Cessna 172 over a boreal forest in Hyytiälä, Finland. The airborne data was complemented by the
450 continuous, comprehensive ground-based measurements at the SMEAR II station.

451

452 We found multiple evidence of nanoparticle layers situated in the topmost part of the RL. Many
453 points would suggest that the particle layers originated from NPF in the upper RL: the particles
454 were in the sub-25 nm size range, the airmasses originated from a sector north-west of Hyytiälä that
455 is associated with NPF and less pollution during non-winter months (Tunved et al., 2006), ground-
456 based observations show continuous growth over several hours indicating a large horizontal source
457 area instead of a point source and increased nucleation rate would be expected to occur in the
458 inversion between RL and FT (Nilsson and Kulmala, 1998). We estimate that such upper RL NPF
459 occurs on 42% of the NPF event days in Hyytiälä. Our results provide new information on NPF in
460 the BL and they should be taken into account when interpreting and analyzing ground-based as well
461 as airborne measurements of aerosol particles.

462

463 **Data availability:** The particle flux and DMPS data can be accessed from <https://avaa.tdata.fi/web/smart/smear> (Junninen et al., 2009; last access: Oct 1, 2020). The BAEC HSRL and radiosonde
464 data is available from <https://adc.arm.gov/discovery/> (Bambha et al., 2014; Keeler et al., 2014); last
465 access: Oct 1, 2020). The Jokioinen soundings can be accessed using the Finnish Meteorological
466 Institute's open data service <https://en.ilmatieteentaitos.fi/open-data> (last access: Oct 1, 2020). The
467 ERA5 dataset can be accessed from <https://cds.climate.copernicus.eu/cdsapp#!/home> (last access:
468 May 6, 2020). The rest of the data was gathered into a dataset that can be accessed from
469 <https://zenodo.org/record/4063662#.X3cHQnUzY88> (Lampilahti et al., 2020; last access: Oct 2,
470 2020).

471

472
473 **Author contribution:** JL, KL, AM, PP, AF, MP, PH, LD and LQ conducted the airborne
474 measurements in 2017. PP wrote processing script for the airborne data. RÖ classified the SMEAR
475 II data for NPF events between 2013-2017. LB, SZ, VMK, TP and MK contributed to the data
476 analysis. YZ and ME analyzed the airborne data between 2011-2018. VV provided the Doppler lidar
477 data. JL prepared the manuscript with contributions from all co-authors.

479 **Acknowledgements:** This project has received funding from the ERC advanced grant No. 742206,
480 the European Union's Horizon 2020 research and innovation program under grant agreement No.
481 654109, the Academy of Finland Center of Excellence project No. 272041 and from the Academy
482 of Finland grant 314 798/799. We thank Erkki Järvinen and the pilots at Airspark Oy for operating
483 the research airplane and we are grateful for their hospitality and helpfulness.

484

485 **References**

486

Aalto, P., Hämeri, K., Becker, E., Weber, R., Salm, J., Mäkelä, J. M., Hoell, C., O'Dowd, C. D., Hansson, H.-C., Väkevä, M., Koponen, I. K., Buzorius, G., and Kulmala, M.: Physical characterization of aerosol particles during nucleation events, *Tellus B*, 53, 344–358, <https://doi.org/10.3402/tellusb.v53i4.17127>, 2001.

Bambha, R., Eloranta, E., Garcia, J., Ermold, B., and Goldsmith, J.: High Spectral Resolution Lidar (HSRL), *Atmospheric Radiat. Meas. ARM User Facil.*, <https://doi.org/10.5439/1025200>, 2014.

Beck, L., Lampilahti, J., Junninen, H., Schobesberger, S., Manninen, A., Leino, K., Quéléver, L., Dada, L., Pullinen, I., Korhonen, F., Bianchi, F., Petäjä, T., Kulmala, M., and Duplissy, J.: Chemical characterisation of negative ions above boreal forest: From ground to free troposphere, in preparation.

Bianchi, F., Tröstl, J., Junninen, H., Frege, C., Henne, S., Hoyle, C. R., Molteni, U., Herrmann, E., Adamov, A., Bukowiecki, N., Chen, X., Duplissy, J., Gysel, M., Hutterli, M., Kangasluoma, J., Kontkanen, J., Kürten, A., Manninen, H. E., Münch, S., Peräkylä, O., Petäjä, T., Rondo, L., Williamson, C., Weingartner, E., Curtius, J., Worsnop, D. R., Kulmala, M., Dommen, J., and Baltensperger, U.: New particle formation in the free troposphere: A question of chemistry and timing, *Science*, aad5456, <https://doi.org/10.1126/science.aad5456>, 2016.

Boucher, O., Randall, D., Artaxo, P., Bretherton, C., Feingold, G., Forster, P., Kerminen, V.-M., Kondo, Y., Liao, H., Lohmann, U., Rasch, P., Satheesh, S. K., Sherwood, S., Stevens, B., and Zhang, X. Y.: Clouds and Aerosols, in: *Climate Change 2013: The Physical Science Basis. Contribution of Working Group I to the Fifth Assessment Report of the Intergovernmental Panel on Climate Change*, edited by: Stocker, T. F., Qin, D., Plattner, G.-K., Tignor, M., Allen, S. K., Boschung, J., Nauels, A., Xia, Y., Bex, V., and Midgley, P. M., Cambridge University Press, Cambridge, United Kingdom and New York, NY, USA, 571–658, 2013.

Boulon, J., Sellegri, K., Hervo, M., Picard, D., Pichon, J.-M., Fréville, P., and Laj, P.: Investigation of nucleation events vertical extent: a long term study at two different altitude sites, *Atmospheric Chem. Phys.*, 11, 5625–5639, <https://doi.org/10.5194/acp-11-5625-2011>, 2011.

Boy, M., Petäjä, T., Dal Maso, M., Rannik, Ü., Rinne, J., Aalto, P., Laaksonen, A., Vaattovaara, P., Joutsensaari, J., Hoffmann, T., Warnke, J., Apostolaki, M., Stephanou, E. G., Tzapakis, M., Kouvarakis, A., Pio, C., Carvalho, A., Römpf, A., Moortgat, G., Spirig, C., Guenther, A., Greenberg, J., Ciccioli, P., and Kulmala, M.: Overview of the field measurement campaign in Hyytiälä, August 2001 in the framework of the EU project OSOA, *Atmospheric Chem. Phys.*, 4, 657–678, <https://doi.org/10.5194/acp-4-657-2004>, 2004.

- Brines, M., Dall'Osto, M., Beddows, D. C. S., Harrison, R. M., Gómez-Moreno, F., Núñez, L., Artúñano, B., Costabile, F., Gobbi, G. P., Salimi, F., Morawska, L., Sioutas, C., and Querol, X.: Traffic and nucleation events as main sources of ultrafine particles in high-insolation developed world cities, *Atmospheric Chem. Phys.*, 15, 5929–5945, <https://doi.org/10.5194/acp-15-5929-2015>, 2015.
- Buenrostro Mazon, S., Riipinen, I., Schultz, D. M., Valtanen, M., Maso, M. D., Sogacheva, L., Junninen, H., Nieminen, T., Kerminen, V.-M., and Kulmala, M.: Classifying previously undefined days from eleven years of aerosol-particle-size distribution data from the SMEAR II station, Hyytiälä, Finland, *Atmospheric Chem. Phys.*, 9, 667–676, <https://doi.org/10.5194/acp-9-667-2009>, 2009.
- Buzorius, G., Rannik, Ü., Mäkelä, J. M., Keronen, P., Vesala, T., and Kulmala, M.: Vertical aerosol fluxes measured by the eddy covariance method and deposition of nucleation mode particles above a Scots pine forest in southern Finland, *J. Geophys. Res. Atmospheres*, 105, 19905–19916, <https://doi.org/10.1029/2000JD900108>, 2000.
- Chen, H., Hodshire, A. L., Ortega, J., Greenberg, J., McMurry, P. H., Carlton, A. G., Pierce, J. R., Hanson, D. R., and Smith, J. N.: Vertically resolved concentration and liquid water content of atmospheric nanoparticles at the US DOE Southern Great Plains site, *Atmospheric Chem. Phys.*, 18, 311–326, <https://doi.org/10.5194/acp-18-311-2018>, 2018.
- Clarke, A. D. and Kapustin, V. N.: A Pacific Aerosol Survey. Part I: A Decade of Data on Particle Production, Transport, Evolution, and Mixing in the Troposphere, *J. Atmospheric Sci.*, 59, 363–382, [https://doi.org/10.1175/1520-0469\(2002\)059<0363:APASPI>2.0.CO;2](https://doi.org/10.1175/1520-0469(2002)059<0363:APASPI>2.0.CO;2), 2002.
- Dada, L., Chellapermal, R., Buenrostro Mazon, S., Paasonen, P., Lampilahti, J., Manninen, H. E., Junninen, H., Petäjä, T., Kerminen, V.-M., and Kulmala, M.: Refined classification and characterization of atmospheric new-particle formation events using air ions, *Atmospheric Chem. Phys.*, 18, 17883–17893, <https://doi.org/10.5194/acp-18-17883-2018>, 2018.
- Dal Maso, M., Kulmala, M., Riipinen, I., Wagner, R., Hussein, T., Aalto, P. P., and Lehtinen, K. E.: Formation and growth of fresh atmospheric aerosols: eight years of aerosol size distribution data from SMEAR II, Hyytiälä, Finland, *Boreal Environ. Res.*, 10, 323, 2005.
- Dunne, E. M., Gordon, H., Kürten, A., Almeida, J., Duplissy, J., Williamson, C., Ortega, I. K., Pringle, K. J., Adamov, A., Baltensperger, U., Barmet, P., Benduhn, F., Bianchi, F., Breitenlechner, M., Clarke, A., Curtius, J., Dommen, J., Donahue, N. M., Ehrhart, S., Flagan, R. C., Franchin, A., Guida, R., Hakala, J., Hansel, A., Heinritzi, M., Jokinen, T., Kangasluoma, J., Kirkby, J., Kulmala, M., Kupc, A., Lawler, M. J., Lehtipalo, K., Makhmutov, V., Mann, G., Mathot, S., Merikanto, J., Miettinen, P., Nenes, A., Onnela, A., Rap, A., Reddington, C. L. S., Riccobono, F., Richards, N. A. D., Rissanen, M. P., Rondo, L., Sarnela, N., Schobesberger, S., Sengupta, K., Simon, M., Sipilä, M., Smith, J. N., Stozkhov, Y., Tomé, A., Tröstl, J., Wagner, P. E., Wimmer, D., Winkler, P. M., Worsnop, D. R., and Carslaw, K. S.: Global atmospheric particle formation from CERN CLOUD measurements, *Science*, 354, 1119–1124, <https://doi.org/10.1126/science.aaf2649>, 2016.
- Gordon, H., Kirkby, J., Baltensperger, U., Bianchi, F., Breitenlechner, M., Curtius, J., Dias, A., Dommen, J., Donahue, N. M., Dunne, E. M., Duplissy, J., Ehrhart, S., Flagan, R. C., Frege, C., Fuchs, C., Hansel, A., Hoyle, C. R., Kulmala, M., Kürten, A., Lehtipalo, K., Makhmutov, V., Molteni, U., Rissanen, M. P., Stozkhov, Y., Tröstl, J., Tsagkogeorgas, G., Wagner, R., Williamson, C., Wimmer, D., Winkler, P. M., Yan, C., and Carslaw, K. S.: Causes and importance of new particle

formation in the present-day and preindustrial atmospheres, *J. Geophys. Res. Atmospheres*, 122, 8739–8760, <https://doi.org/10.1002/2017JD026844>, 2017.

Größ, J., Hamed, A., Sonntag, A., Spindler, G., Manninen, H. E., Nieminen, T., Kulmala, M., Hörrak, U., Plass-Dülmer, C., Wiedensohler, A., and Birmili, W.: Atmospheric new particle formation at the research station Melpitz, Germany: connection with gaseous precursors and meteorological parameters, *Atmospheric Chem. Phys.*, 18, 1835–1861, <https://doi.org/10.5194/acp-18-1835-2018>, 2018.

Hari, P. and Kulmala, M.: Station for measuring ecosystem-atmosphere relations (SMEAR II), *Boreal Environ. Res.*, 10, 315–322, 2005.

Junkermann, W. and Hacker, J. M.: Ultrafine Particles in the Lower Troposphere: Major Sources, Invisible Plumes, and Meteorological Transport Processes, *Bull. Am. Meteorol. Soc.*, 99, 2587–2602, <https://doi.org/10.1175/BAMS-D-18-0075.1>, 2018.

Junninen, H., Lauri, A., Keronen, P., Aalto, P., Hiitonen, V., Hari, P., and Kulmala, M.: Smart-SMEAR: on-line data exploration and visualization tool for SMEAR stations., *Boreal Environ. Res.*, 14, 447–457, 2009.

Keeler, E., Coulter, R., Kyrouac, J., and Holdridge, D.: Balloon-Borne Sounding System (SONDEWNP), *Atmospheric Radiat. Meas. ARM User Facil.*, <https://doi.org/10.5439/1021460>, 2014.

Kerminen, V.-M., Chen, X., Vakkari, V., Petäjä, T., Kulmala, M., and Bianchi, F.: Atmospheric new particle formation and growth: review of field observations, *Environ. Res. Lett.*, 13, 103003, <https://doi.org/10.1088/1748-9326/aadf3c>, 2018.

Kulmala, M., Vehkamäki, H., Petäjä, T., Dal Maso, M., Lauri, A., Kerminen, V.-M., Birmili, W., and McMurry, P. H.: Formation and growth rates of ultrafine atmospheric particles: a review of observations, *J. Aerosol Sci.*, 35, 143–176, <https://doi.org/10.1016/j.jaerosci.2003.10.003>, 2004.

Kulmala, M., Petäjä, T., Nieminen, T., Sipilä, M., Manninen, H. E., Lehtipalo, K., Dal Maso, M., Aalto, P. P., Junninen, H., Paasonen, P., Riipinen, I., Lehtinen, K. E. J., Laaksonen, A., and Kerminen, V.-M.: Measurement of the nucleation of atmospheric aerosol particles, *Nat. Protoc.*, 7, 1651–1667, <https://doi.org/10.1038/nprot.2012.091>, 2012.

Laakso, L., Grönholm, T., Kulmala, L., Haapanala, S., Hirsikko, A., Lovejoy, E. R., Kazil, J., Kurten, T., Boy, M., Nilsson, E. D., Sogachev, A., Riipinen, I., Stratmann, F., and Kulmala, M.: Hot-air balloon as a platform for boundary layer profile measurements during particle formation, *Boreal Environ. Res.*, 12, 279–294, 2007.

Lampilahti, J., Leino, K., Manninen, A., Poutanen, P., Franck, A., Peltola, M., Hietala, P., Beck, L., Dada, L., Quéléver, L., Öhrnberg, R., Zhou, Y., Ekblom, M., Vakkari, V., Zilitinkevich, S., Kerminen, V.-M., Petäjä, T., and Kulmala, M.: Aerosol particle formation in the upper residual layer: dataset, <https://doi.org/10.5281/zenodo.4063662>, 2020.

Leino, K., Lampilahti, J., Poutanen, P., Väänänen, R., Manninen, A., Buenrostro Mazon, S., Dada, L., Franck, A., Wimmer, D., Aalto, P. P., Ahonen, L. R., Enroth, J., Kangasluoma, J., Keronen, P., Korhonen, F., Laakso, H., Matilainen, T., Siivola, E., Manninen, H. E., Lehtipalo, K., Kerminen, V.-M., Petäjä, T., and Kulmala, M.: Vertical profiles of sub-3 nm particles over the boreal forest, *Atmospheric Chem. Phys.*, 19, 4127–4138, <https://doi.org/10.5194/acp-19-4127-2019>, 2019.

- Manninen, H. E., Petäjä, T., Asmi, E., Riipinen, N., Nieminen, T., Mikkilä, J., Horrak, U., Mirme, A., Mirme, S., Laakso, L., Kerminen, V.-M., and Kulmala, M.: Long-term field measurements of charged and neutral clusters using Neutral cluster and Air Ion Spectrometer (NAIS), *Boreal Environ. Res.*, 14, 591–605, 2009.
- Meskhidze, N., Jaimes-Correa, J. C., Petters, M. D., Royalty, T. M., Phillips, B. N., Zimmerman, A., and Reed, R.: Possible Wintertime Sources of Fine Particles in an Urban Environment, *J. Geophys. Res. Atmospheres*, 124, 13055–13070, <https://doi.org/10.1029/2019JD031367>, 2019.
- Mirme, S. and Mirme, A.: The mathematical principles and design of the NAIS – a spectrometer for the measurement of cluster ion and nanometer aerosol size distributions, *Atmospheric Meas. Tech.*, 6, 1061–1071, <https://doi.org/10.5194/amt-6-1061-2013>, 2013.
- Nieminen, T., Asmi, A., Dal Maso, M., Aalto, P. P., Keronen, P., Petäjä, T., Kulmala, M., and Kerminen, V.-M.: Trends in atmospheric new-particle formation: 16 years of observations in a boreal-forest environment, *Boreal Environ. Res.*, 19, 191–214, 2014.
- Nikandrova, A., Tabakova, K., Manninen, A., Väänänen, R., Petäjä, T., Kulmala, M., Kerminen, V.-M., and O'Connor, E.: Combining airborne in situ and ground-based lidar measurements for attribution of aerosol layers, *Atmospheric Chem. Phys.*, 18, 10575–10591, <https://doi.org/10.5194/acp-18-10575-2018>, 2018.
- Nilsson, E. D. and Kulmala, M.: The potential for atmospheric mixing processes to enhance the binary nucleation rate, *J. Geophys. Res. Atmospheres*, 103, 1381–1389, <https://doi.org/10.1029/97JD02629>, 1998.
- Nilsson, E. D., Rannik, Ü., Kulmala, M., Buzorius, G., and O’Dowd, C. D.: Effects of continental boundary layer evolution, convection, turbulence and entrainment, on aerosol formation, *Tellus B*, 53, 441–461, <https://doi.org/10.1034/j.1600-0889.2001.530409.x>, 2001.
- O’Connor, E. J., Illingworth, A. J., Brooks, I. M., Westbrook, C. D., Hogan, R. J., Davies, F., and Brooks, B. J.: A Method for Estimating the Turbulent Kinetic Energy Dissipation Rate from a Vertically Pointing Doppler Lidar, and Independent Evaluation from Balloon-Borne In Situ Measurements, *J. Atmospheric Ocean. Technol.*, 27, 1652–1664, <https://doi.org/10.1175/2010JTECHA1455.1>, 2010.
- O’Dowd, C. D., Yoon, Y. J., Junkermann, W., Aalto, P., Kulmala, M., Lihavainen, H., and Viisanen, Y.: Airborne measurements of nucleation mode particles II: boreal forest nucleation events, *Atmospheric Chem. Phys.*, 9, 937–944, <https://doi.org/10.5194/acp-9-937-2009>, 2009.
- Pearson, G., Davies, F., and Collier, C.: An Analysis of the Performance of the UFAM Pulsed Doppler Lidar for Observing the Boundary Layer, *J. Atmospheric Ocean. Technol.*, 26, 240–250, <https://doi.org/10.1175/2008JTECHA1128.1>, 2009.
- Petäjä, T., O’Connor, E. J., Moisseev, D., Sinclair, V. A., Manninen, A. J., Väänänen, R., von Lerber, A., Thornton, J. A., Nicoll, K., Petersen, W., Chandrasekar, V., Smith, J. N., Winkler, P. M., Krüger, O., Hakola, H., Timonen, H., Brus, D., Laurila, T., Asmi, E., Riekkola, M.-L., Mona, L., Massoli, P., Engelmann, R., Komppula, M., Wang, J., Kuang, C., Bäck, J., Virtanen, A., Levula, J., Ritsche, M., and Hickmon, N.: BAEC: A Field Campaign to Elucidate the Impact of Biogenic Aerosols on Clouds and Climate, *Bull. Am. Meteorol. Soc.*, 97, 1909–1928, <https://doi.org/10.1175/BAMS-D-14-00199.1>, 2016.

- Pierce, J. R. and Adams, P. J.: Uncertainty in global CCN concentrations from uncertain aerosol nucleation and primary emission rates, *Atmospheric Chem. Phys.*, 9, 1339–1356, <https://doi.org/10.5194/acp-9-1339-2009>, 2009.
- Platis, A., Altstädter, B., Wehner, B., Wildmann, N., Lampert, A., Hermann, M., Birmili, W., and Bange, J.: An Observational Case Study on the Influence of Atmospheric Boundary-Layer Dynamics on New Particle Formation, *Bound.-Layer Meteorol.*, 158, 67–92, <https://doi.org/10.1007/s10546-015-0084-y>, 2015.
- Posner, L. N. and Pandis, S. N.: Sources of ultrafine particles in the Eastern United States, *Atmos. Environ.*, 111, 103–112, <https://doi.org/10.1016/j.atmosenv.2015.03.033>, 2015.
- Rose, C., Sellegri, K., Moreno, I., Velarde, F., Ramonet, M., Weinhold, K., Krejci, R., Andrade, M., Wiedensohler, A., Ginot, P., and Laj, P.: CCN production by new particle formation in the free troposphere, *Atmospheric Chem. Phys.*, 17, 1529–1541, <https://doi.org/10.5194/acp-17-1529-2017>, 2017.
- Salma, I., Varga, V., and Németh, Z.: Quantification of an atmospheric nucleation and growth process as a single source of aerosol particles in a city, *Atmospheric Chem. Phys.*, 17, 15007–15017, <https://doi.org/10.5194/acp-17-15007-2017>, 2017.
- Schobesberger, S., Väänänen, R., Leino, K., Virkkula, A., Backman, J., Pohja, T., Siivola, E., Franchin, A., Mikkilä, J., Paramonov, M., Aalto, P. P., Krejci, R., Petäjä, T., and Kulmala, M.: Airborne measurements over the boreal forest of southern Finland during new particle formation events in 2009 and 2010, *Boreal Environ. Res.*, 18, 145–164, 2013.
- Siebert, H., Stratmann, F., and Wehner, B.: First observations of increased ultrafine particle number concentrations near the inversion of a continental planetary boundary layer and its relation to ground-based measurements, *Geophys. Res. Lett.*, 31, L09102, <https://doi.org/10.1029/2003GL019086>, 2004.
- Stanier, C. O., Khlystov, A. Y., and Pandis, S. N.: Nucleation Events During the Pittsburgh Air Quality Study: Description and Relation to Key Meteorological, Gas Phase, and Aerosol Parameters Special Issue of Aerosol Science and Technology on Findings from the Fine Particulate Matter Supersites Program, *Aerosol Sci. Technol.*, 38, 253–264, <https://doi.org/10.1080/02786820390229570>, 2004.
- Stratmann, F., Siebert, H., Spindler, G., Wehner, B., Althausen, D., Heintzenberg, J., Hellmuth, O., Rinke, R., Schmieder, U., Seidel, C., Tuch, T., Uhrner, U., Wiedensohler, A., Wandinger, U., Wendisch, M., Schell, D., and Stohl, A.: New-particle formation events in a continental boundary layer: first results from the SATURN experiment, *Atmospheric Chem. Phys.*, 3, 1445–1459, <https://doi.org/10.5194/acp-3-1445-2003>, 2003.
- Stull, R. B.: *An Introduction to Boundary Layer Meteorology*, Softcover reprint of the original 1st ed. 1988 edition., Springer, Dordrecht, 670 pp., 1988.
- Takegawa, N., Moteki, N., Oshima, N., Koike, M., Kita, K., Shimizu, A., Sugimoto, N., and Kondo, Y.: Variability of aerosol particle number concentrations observed over the western Pacific in the spring of 2009, *J. Geophys. Res. Atmospheres*, 119, 13,474–13,488, <https://doi.org/10.1002/2014JD022014>, 2014.

Tunved, P., Hansson, H.-C., Kerminen, V.-M., Ström, J., Maso, M. D., Lihavainen, H., Viisanen, Y., Aalto, P. P., Komppula, M., and Kulmala, M.: High Natural Aerosol Loading over Boreal Forests, *Science*, 312, 261–263, <https://doi.org/10.1126/science.1123052>, 2006.

Väänänen, R., Krejci, R., Manninen, H. E., Manninen, A., Lampilahti, J., Buenrostro Mazon, S., Nieminen, T., Yli-Juuti, T., Kontkanen, J., Asmi, A., Aalto, P. P., Keronen, P., Pohja, T., O'Connor, E., Kerminen, V.-M., Petäjä, T., and Kulmala, M.: Vertical and horizontal variation of aerosol number size distribution in the boreal environment, *Atmospheric Chem. Phys. Discuss.*, Manuscript in review, <https://doi.org/10.5194/acp-2016-556>, 2016.

Vakkari, V., Manninen, A. J., O'Connor, E. J., Schween, J. H., Zyl, P. G. van, and Marinou, E.: A novel post-processing algorithm for Halo Doppler lidars, *Atmospheric Meas. Tech.*, 12, 839–852, <https://doi.org/10.5194/amt-12-839-2019>, 2019.

Venzac, H., Sellegri, K., Laj, P., Villani, P., Bonasoni, P., Marinoni, A., Cristofanelli, P., Calzolari, F., Fuzzi, S., Decesari, S., Facchini, M.-C., Vuillermoz, E., and Verza, G. P.: High frequency new particle formation in the Himalayas, *Proc. Natl. Acad. Sci.*, 105, 15666–15671, <https://doi.org/10.1073/pnas.0801355105>, 2008.

Wang, J., Krejci, R., Giangrande, S., Kuang, C., Barbosa, H. M. J., Brito, J., Carbone, S., Chi, X., Comstock, J., Ditas, F., Lavric, J., Manninen, H. E., Mei, F., Moran-Zuloaga, D., Pöhlker, C., Pöhlker, M. L., Saturno, J., Schmid, B., Souza, R. A. F., Springston, S. R., Tomlinson, J. M., Toto, T., Walter, D., Wimmer, D., Smith, J. N., Kulmala, M., Machado, L. A. T., Artaxo, P., Andreae, M. O., Petäjä, T., and Martin, S. T.: Amazon boundary layer aerosol concentration sustained by vertical transport during rainfall, *Nature*, 539, 416–419, <https://doi.org/10.1038/nature19819>, 2016.

Wehner, B., Siebert, H., Ansmann, A., Ditas, F., Seifert, P., Stratmann, F., Wiedensohler, A., Apituley, A., Shaw, R. A., Manninen, H. E., and Kulmala, M.: Observations of turbulence-induced new particle formation in the residual layer, *Atmospheric Chem. Phys.*, 10, 4319–4330, <https://doi.org/10.5194/acp-10-4319-2010>, 2010.

Williamson, C. J., Kupc, A., Axisa, D., Bilsback, K. R., Bui, T., Campuzano-Jost, P., Dollner, M., Froyd, K. D., Hodshire, A. L., Jimenez, J. L., Kodros, J. K., Luo, G., Murphy, D. M., Nault, B. A., Ray, E. A., Weinzierl, B., Wilson, J. C., Yu, F., Yu, P., Pierce, J. R., and Brock, C. A.: A large source of cloud condensation nuclei from new particle formation in the tropics, *Nature*, 574, 399–403, <https://doi.org/10.1038/s41586-019-1638-9>, 2019.

Yu, F. and Luo, G.: Simulation of particle size distribution with a global aerosol model: contribution of nucleation to aerosol and CCN number concentrations, *Atmospheric Chem. Phys.*, 9, 7691–7710, 2009.

Yu, X., Venecek, M., Kumar, A., Hu, J., Tanrikulu, S., Soon, S.-T., Tran, C., Fairley, D., and Kleeman, M. J.: Regional sources of airborne ultrafine particle number and mass concentrations in California, *Atmospheric Chem. Phys.*, 19, 14677–14702, <https://doi.org/10.5194/acp-19-14677-2019>, 2019.

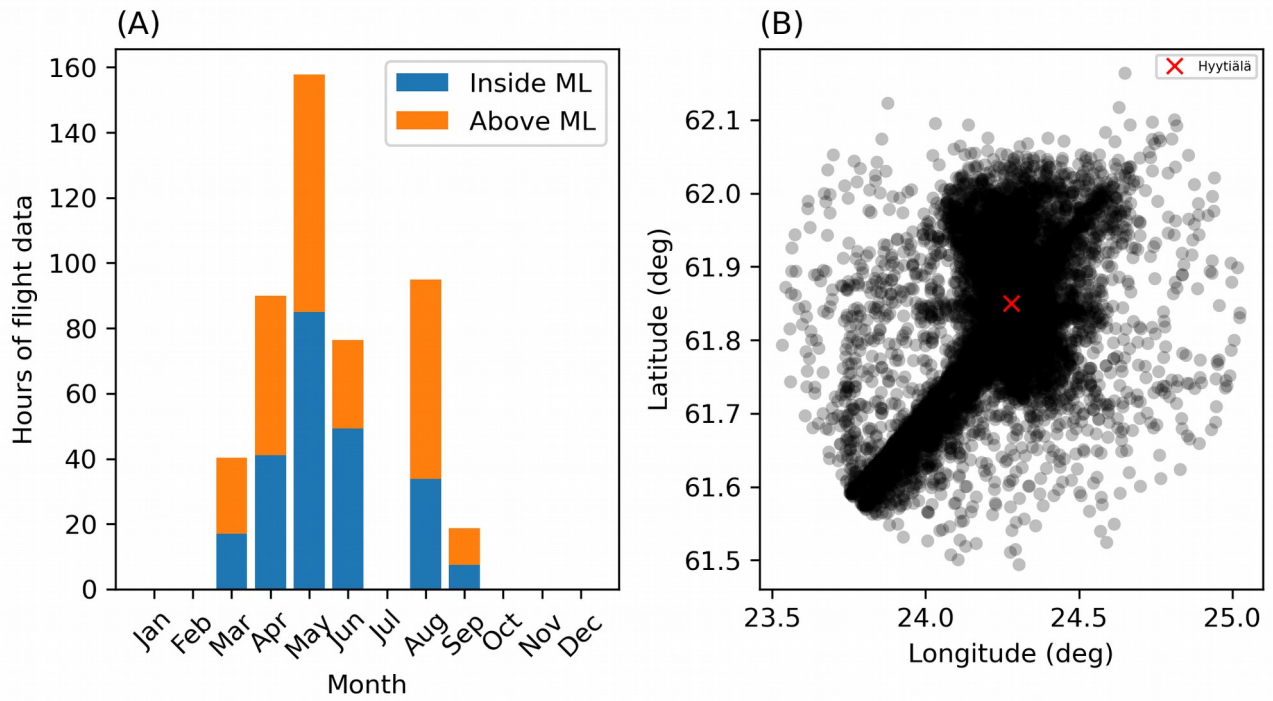


Figure 1: (A) monthly airborne data availability between 2011-2018 divided into measurements above and below the ML, based on the ML height obtained from the ERA5 reanalysis data. (B) horizontal distribution of the 2011-2018 airborne measurement data. We chose the data within 40 km radius from Hyytiälä.

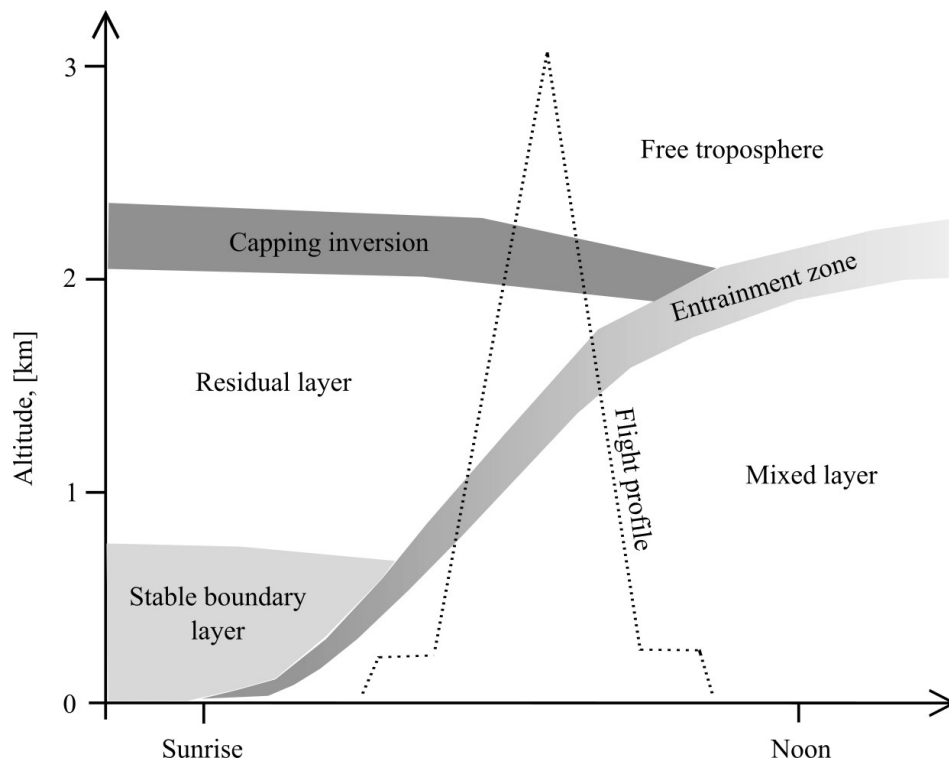


Figure 2: A schematic diagram of an average flight profile in relation to BL evolution.

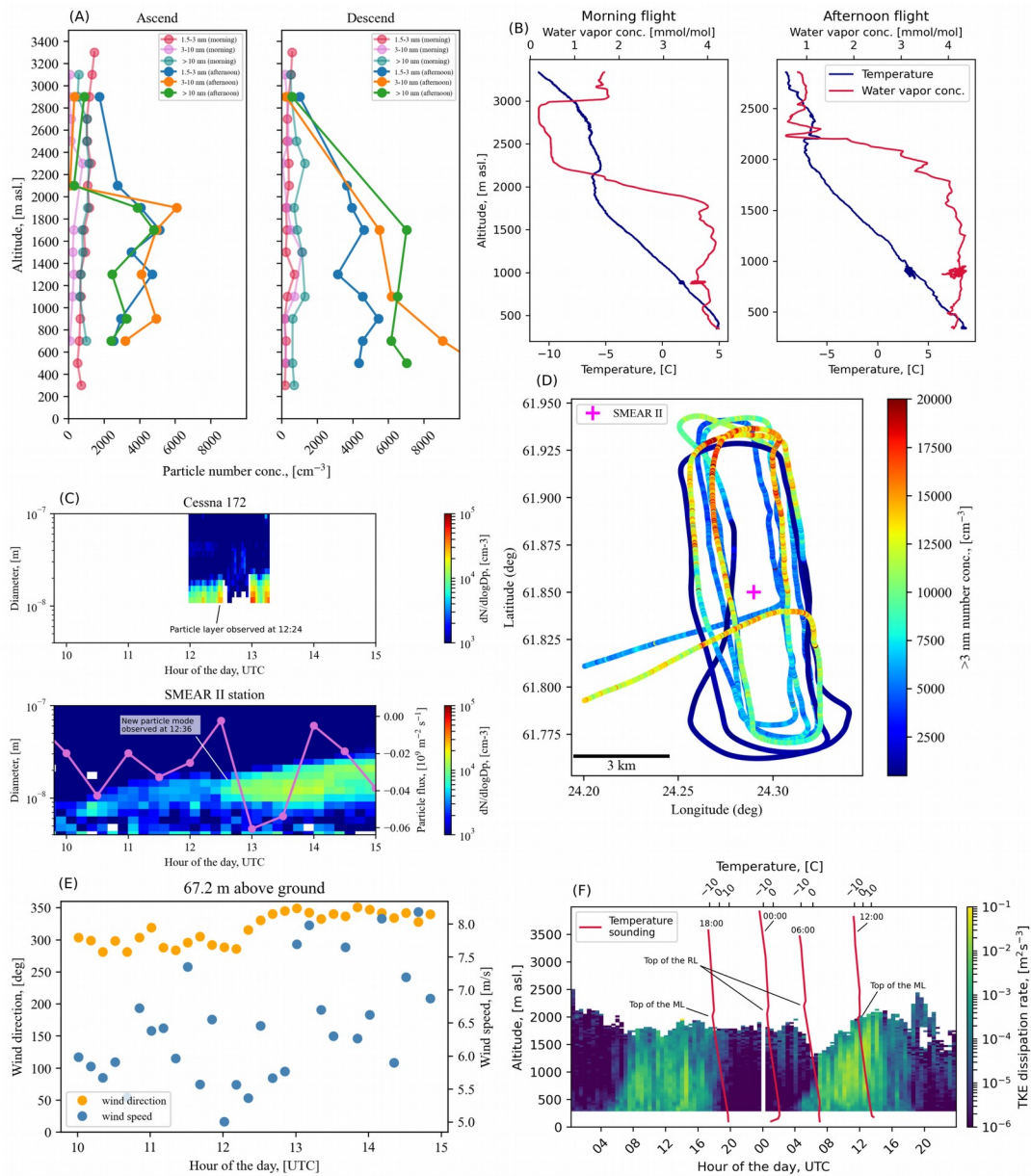


Figure 3: Panel (A) shows vertical profiles of aerosol particle number concentration in three different size ranges (1.5-3 nm, 3-10 nm and >10 nm) on May 2, 2017. The data shows the morning flight (02:26-03:55 UTC) and the afternoon flight (12:00-13:20 UTC). The profile from the afternoon flight is restricted to the northern part of the flight track (E:24.25-24.35, N:61.875-61.95). Panel (B) shows the temperature and water vapor concentration profiles from the morning and the afternoon ascents. Panel (C) shows the particle number-size distribution from the measurement airplane and the SMEAR II station. The vertical flux of >10 nm particles is superimposed. Negative means downward and positive upward particle flux. Panel (D) shows the afternoon flight track colored by >3 nm particle number concentration. Panel (E) shows the wind speed and direction from the SMEAR II mast (67.2 m). Panel (F) shows turbulent kinetic energy (TKE) dissipation rate measured by the Doppler lidar in Hyytiälä between May 1-2, 2017. Temperature soundings from Jokioinen are superimposed.

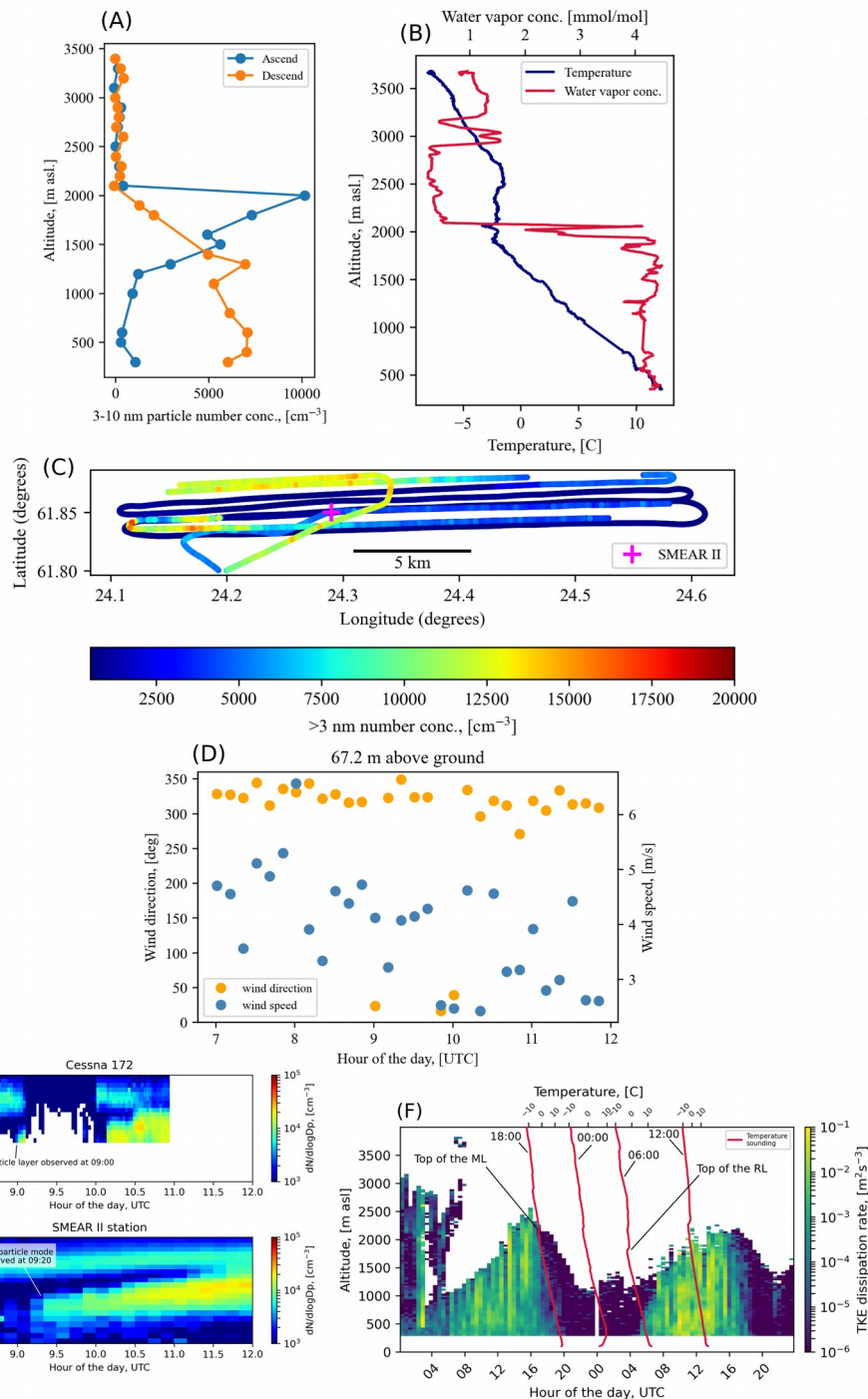


Figure 4: Panel (A) shows vertical profiles of 3-10 nm particle number concentration on May 19, 2017 between 8:42-10:24 UTC. Panel (B) shows the temperature and water vapor concentration profiles during the ascend. Panel (C) shows the afternoon flight track colored by >3 nm particle number concentration. Panel (D) shows the wind direction and speed measured from the SMEAR II mast at 67.2 m. Panel (E) shows the particle number-size distribution from the measurement airplane and the SMEAR II station. Panel (F) shows turbulent kinetic energy (TKE) dissipation rate measured by the Doppler lidar in Hyttiälä between May 18-19, 2018. Temperature soundings from Jokioinen are superimposed.

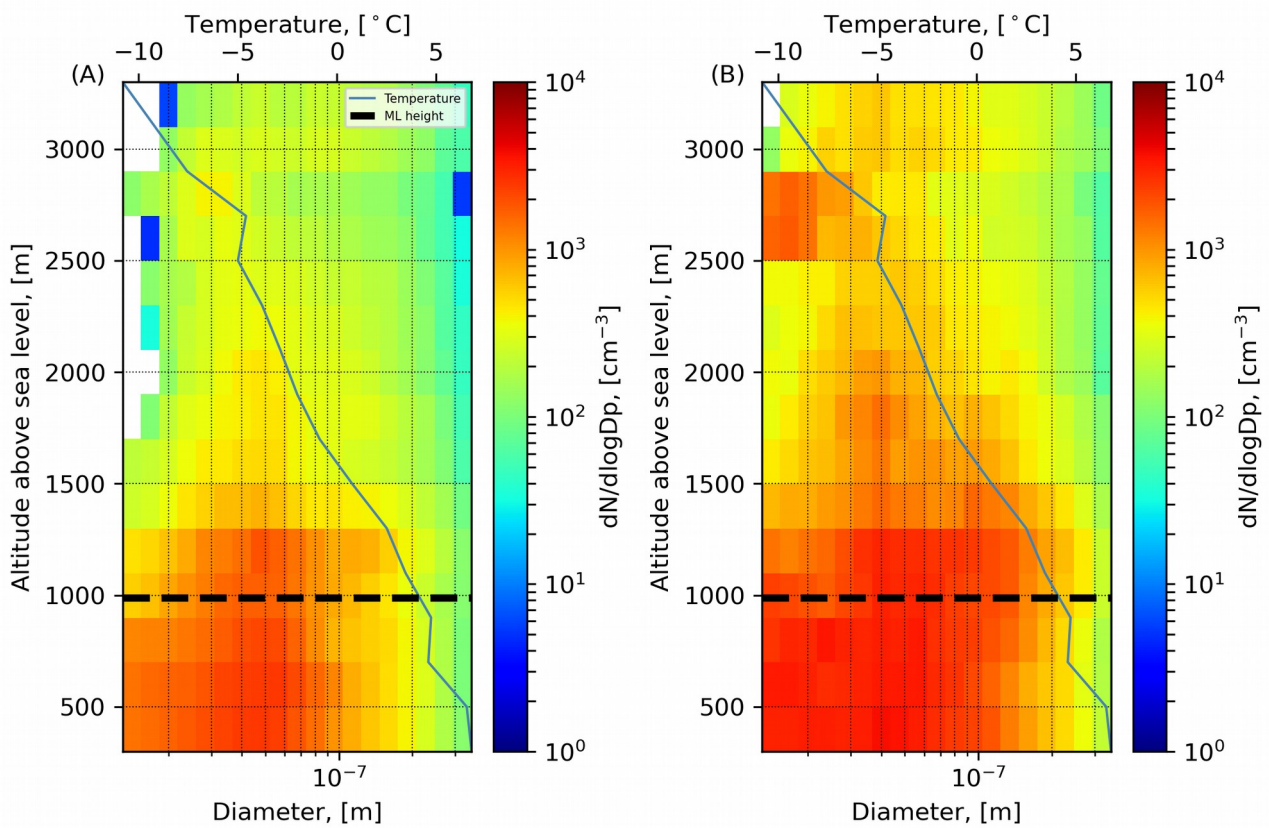


Figure 5: Panel (A) shows the median and panel (B) the 75th percentile vertical profile of particle number-size distribution measured on board the Cessna on NPF event days between 9-12 AM. The number-size distribution was binned into 200 m altitude bins. The data is from the campaigns conducted between 2011-2018. The dashed line is the mean ML height obtained from the ERA5 reanalysis data. The blue line shows the mean temperature profile from measurement flights when the sub-25 nm number concentration in the 2000-3000 m altitude range was above the 75th percentile.

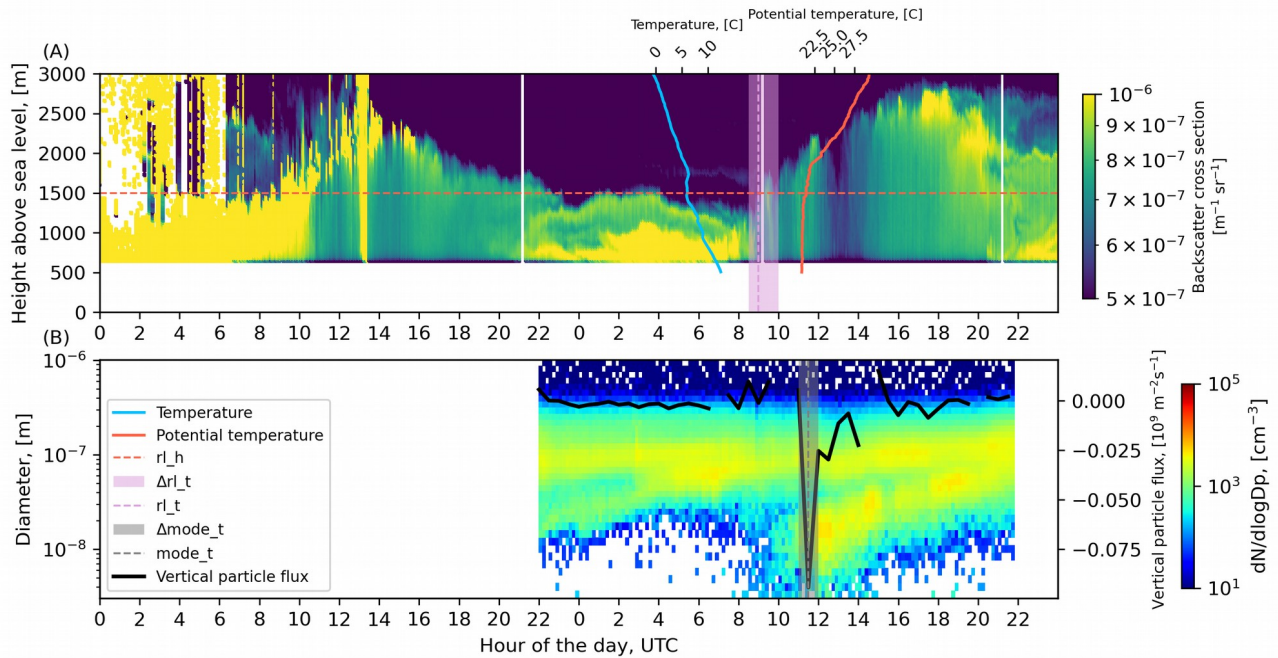


Figure 6: Panel (A) shows the backscatter cross section measured by the HSRL on June 4-5, 2014. The development of the ML is visible from the backscatter cross section signal. Temperature and potential temperature from soundings released in Hyytiälä at 5:20 and 11:20 on June 5, 2014 respectively are superimposed. The horizontal line rl_h refers to the height of the inversion base in the sounding (height of the RL). The rl_t and Δrl_t refer to the time when the ML was estimated to reach the rl_h and the confidence interval for this time, respectively. Panel (B) shows the particle number-size distribution measured at the SMEAR II station, the black line is the vertical particle flux. The $mode_t$ and $\Delta mode_t$ respectively refer to the time and the confidence interval, when a nucleation particle mode that is associated with downward particle flux suddenly appears.

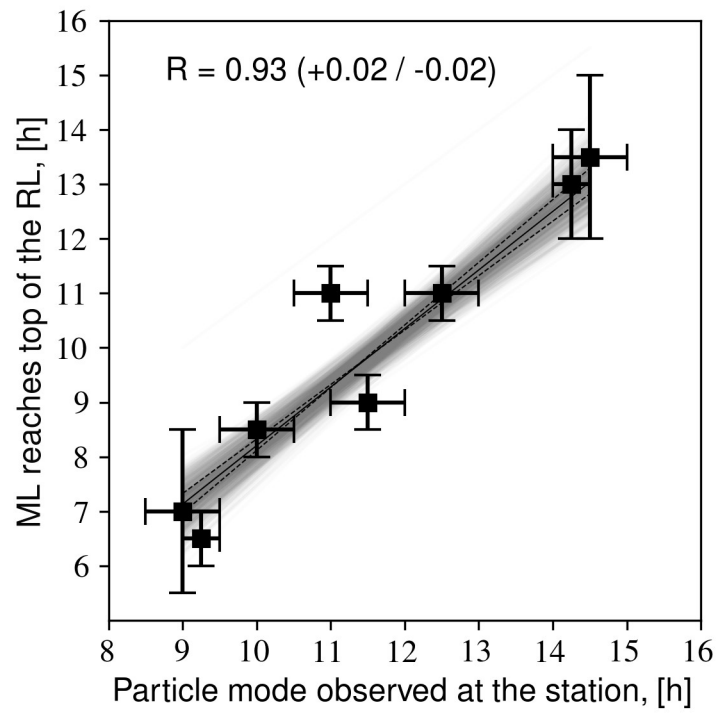


Figure 7: The correlation between the times when a new particle mode coupled with downward particle flux was observed at the field site and the times when the ML reached the top of the RL.

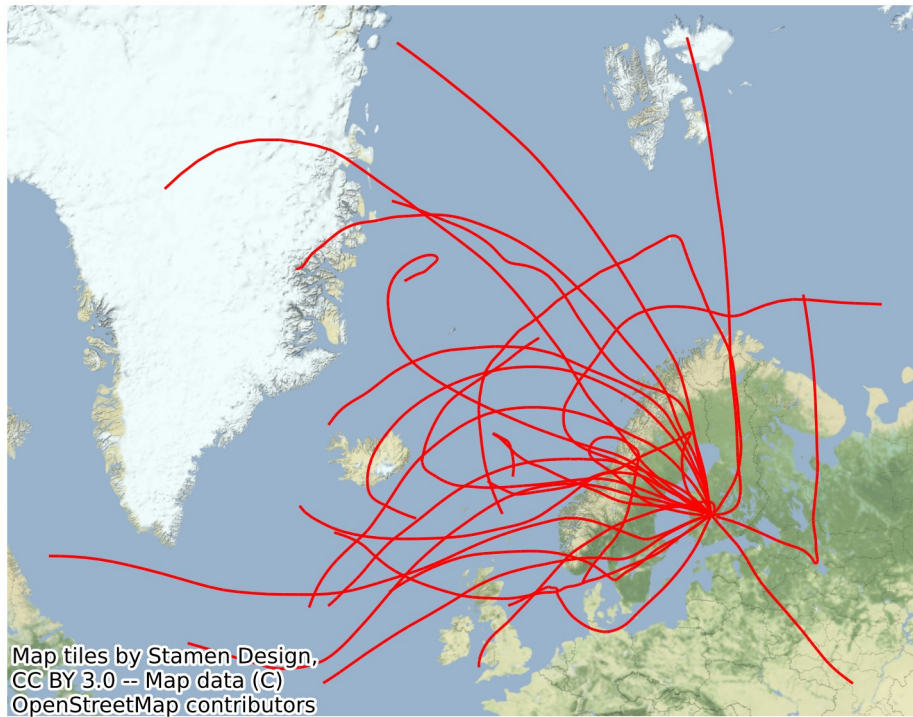


Figure 8: Airmass back trajectories arriving to altitude over Hyytiälä where nucleation mode particle layers were located based on airborne data and the BAEC data. We calculated the airmass histories for 72 hours, however in the figure some of the trajectories are truncated to fit the map. The trajectories were calculated based on two different conditions. First, based on the BAEC data analysis (Section 3.5) such that the airmass arrived at the top of the RL when the ML reached that altitude (see Table 1 for these altitudes and times). Second, based on the vertical profiles between 2011-2018 (Section 3.4) such that the back trajectories arrived at 2600 m altitude at 10:00 UTC on the days when the N_{10-25} in 2000-3000 m altitude range exceeded the 75th percentile N_{10-25} value.

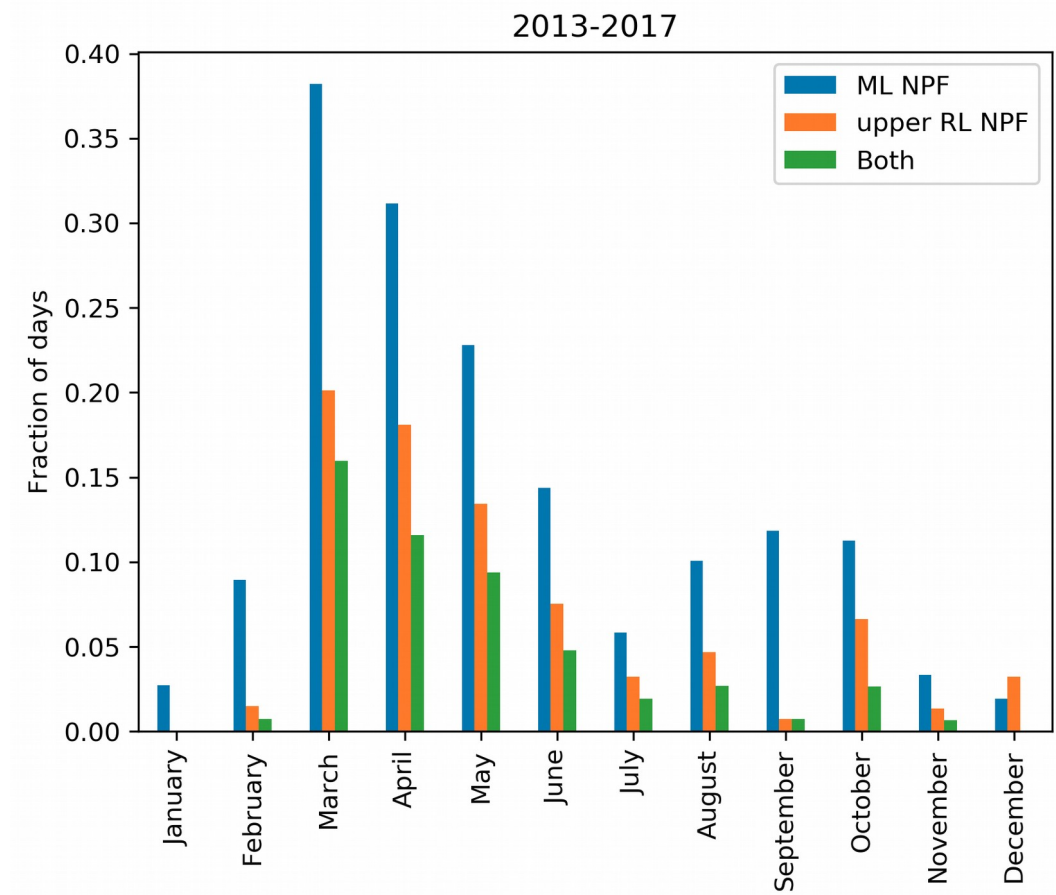


Figure 9: Monthly fractions of NPF within the ML and NPF in the upper RL in Hyytiälä between 2013-2017.

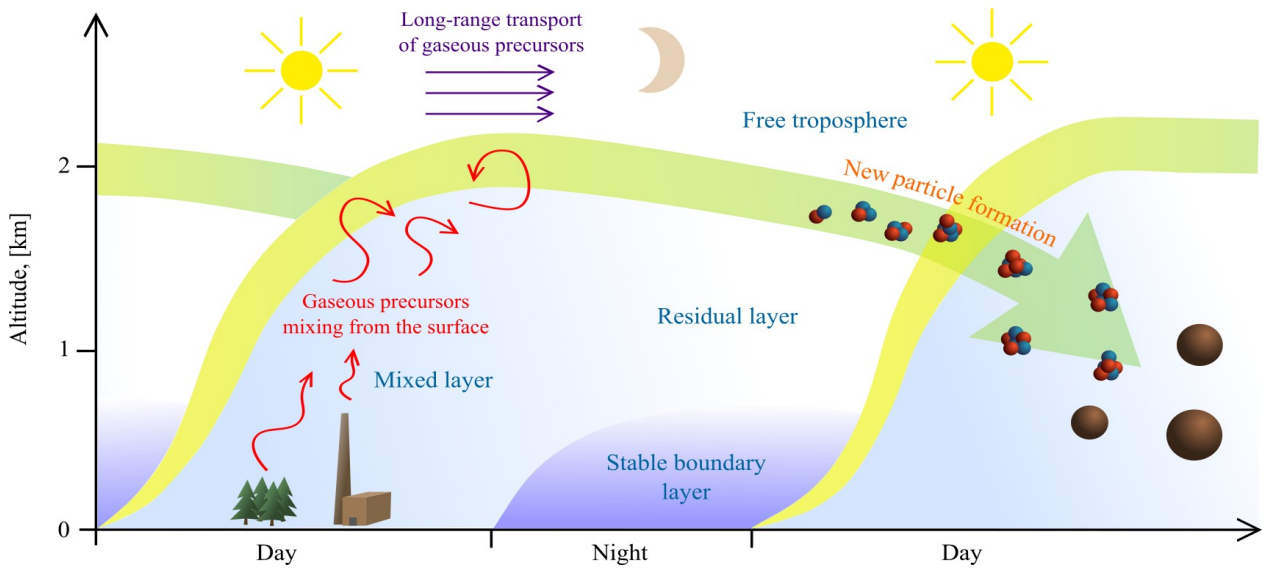


Figure 10: Schematic drawing illustrating the proposed mechanism behind NPF in the upper RL. Gaseous precursors released from biogenic and/or anthropogenic sources are mixed throughout the ML. When the mixing stops during the night the gases are stuck in the RL. Also gaseous precursors may be transported in the FT. In the following morning photochemistry begins and aerosol particles are formed in the interface between the RL and the FT. The freshly formed particles remain in the elevated layer or get mixed into the a new ML if it reaches the height of the upper RL. The aerosol particles continue to grow larger, contributing to the aerosol load in the BL.

Table 1: rl_h = residual layer height during night or early morning (m asl), rl_ht = time when the rl_h was observed (time when the sounding was released, hour of the day, UTC), mode_t = nucleation mode particle mode first appears (hour of the day, UTC), mode_t1/mode_t2 = nucleation mode particle mode appearance confidence interval (hour of the day, UTC), rl_t = new mixed layer reaches the top of the residual layer (hour of the day, UTC), rl_t1/rl_t2 = new mixed layer reaches the top of the residual layer confidence interval (hour of the day, UTC), bl_h = observed maximum height of the previous day's boundary layer (m asl.), dp = mean mode diameter for the newly appeared particle mode, when they first appear (nm), gr = growth rate calculated for the newly appeared particle mode (nm h⁻¹), pf = the value of the negative particle flux peak (10⁹ m⁻² s⁻¹).

date	rl_ht	rl_h	mode_t1	mode_t	mode_t2	rl_t1	rl_t	rl_t2	dp	bl_h	pf	gr
20140328	5.3	1100	8.5	9	9.5	5.5	7	8	20	1300	-0.25	2.28
20140331	7.6	2400	14	14.5	15	12	13.5	14	10	2200	-0.06	2.1
20140404	8.5	2200	10.5	11	11.5	10.5	11	11.5	8	2800	-0.04	1.39
20140409	5.5	1500	9	9.25	9.5	6	6.5	7	8	1800	-0.13	1.18
20140415	5.3	1600	14.5	14.25	15	12	13	14	11	1700	-0.18	1.94
20140422	0.0	1800	12	12.5	13	10.5	11	11.5	17	1900	-0.17	1.0
20140518	0.0	1500	9.5	10	10.5	8	8.5	9	13	1900	-0.11	2.91
20140705	5.3	1500	11	11.5	12	8.5	9	10	12	1700	-0.1	4.83

488